ADVANCED FUNCTIONAL MATERIALS
www.afm-journal.de

Effect of Doping Concentration on Microstructure of Conjugated Polymers and Characteristics in N-Type Polymer Field-Effect Transistors

Chuan Liu, Junhyuk Jang, Yong Xu, Hyo-Jung Kim, Dongyoon Khim, Won-Tae Park, Yong-Young Noh, and Jang-Joo Kim**

Despite extensive progress in organic field-effect transistors, there are still far fewer reliable, high-mobility n-type polymers than p-type polymers. It is demonstrated that by using dopants at a critical doping molar ratio (*MR*), performance of n-type polymer poly[[*N*,*N*9-bis(2-octyldodecyl)-naphthalene-1,4,5,8-bis(dicarboximide)-2,6-diyl]-alt-5,59-(2,29-bithiophene)] (P(NDI2DO-T2)) field-effect transistors (FETs) can be significantly improved and simultaneously optimized in mobility, on–off ratio, crystallinity, injection, and reliability. In particular, when using the organic dopant bis(cyclopentadienyl)–cobalt(II) (cobaltocene, $CoCp_2$) at a low concentration (0.05 wt%), the FET mobility is increased from 0.34 to 0.72 $cm^2\ V^{-1}\ s^{-1}$, and the threshold voltage was decreased from 32.7 to 8.8 V. The relationship between the *MR* of dopants and electrical characteristics as well as the evolution in polymer crystallinity revealed by synchrotron X-ray diffractions are systematically investigated. Deviating from previous discoveries, it is found that mobility increases first and then decreases drastically beyond a critical value of *MR*. Meanwhile, the intensity and width of the main peak of in-plane X-ray diffraction start to decrease at the same critical *MR*. Thus, the mobility decrease is correlated with the disturbed in-plane crystallinity of the conjugated polymer, for both organic and inorganic dopants. The method provides a simple and efficient approach to employing dopants to optimize the electrical performance and microstructure of P(NDI2DO-T2).

1. Introduction

Organic field-effect transistors (OFETs) have recently attracted significant attention because of their high potential in lightweight, flexible, and large-area electronics processed by means of cost-effective graphic art printing processes.[1] Soluble polymeric semiconductors are strong candidates as active layers to realize those devices, since a high-quality thin film can be achieved by various simple coating methods through a stable formulation in various organic solvents.[2,3] Recently, various conjugated polymers have been reported to have high field-effect mobilities of 1.0–23.7 $cm^2\ V^{-1}\ s^{-1}$,[3,4] exceeding those of amorphous silicon field-effect transistors (FETs). Although the values have recently shown rapid progress and they meet the requirement for driving circuits in various display panels, polymeric complementary integrated circuits are still hard to realize due to the lack of balanced n-type components. This is because, generally, n-channel polymers have lower mobility and stability than p-channel polymers, owing to the difficulty of material synthesis of the deep-lying lowest unoccupied molecular orbital (LUMO) located near 3.6–4.5 eV as well as the abundant trap sites generated by hydrogenated oxygen.[5]

Polymers with strong electron-accepting naphthalene-bis(dicarboximide) (NDI) cores are promising materials for high performance and operational stability in n-channel operation. Poly[[*N*,*N*9-bis(2-octyldodecyl)-naphthalene-1,4,5,8-bis(dicarboximide)-2,6-diyl]-alt-5,59-(2,29-bithiophene)] (P(NDI2DO-T2), Polyera Activink N2200)[6,7] and poly[(E)-2,7-bis(2-decyltetradecyl)-4-methyl-9-(5-(2-(5-methylthiophen-2-yl)vinyl)thophen-2-yl)benzo[lmn][3,8]phenanthoroline-1,3,6,8(2H,7H)-tetraone] (PNDI-TVT)[8] were reported to achieve electron mobilities of 0.85 and 1.8 $cm^2\ V^{-1}\ s^{-1}$, respectively. The large and planar conjugated bicyclic structure, with its strong π–π interaction, facilitates electron transport through interchain hopping, and the electron-withdrawing diimide group for each naphthalene moiety effectively pulls down the LUMO level, affording good air stability.[8] However, compared

Prof. C. Liu
State Key Laboratory of Optoelectronic Materials and Technologies
School of Physics and Engineering
Sun Yat-Sen University
Guangzhou 510274, China
Prof. C. Liu, Prof. Y. Xu, Dr. D. Khim, W.-T. Park, Prof. Y.-Y. Noh
Department of Energy and Materials Engineering
Dongguk University
26, Pil-dong, 3-ga, Jung-gu, Seoul 100-715, Republic of Korea
E-mail: yynoh@dongguk.edu
Dr. J. Jang, Prof. J.-J. Kim
Department of Materials Science and Engineering
Seoul National University
599, Gwanak-ro, Gwanak-gu, Seoul, Republic of Korea
E-mail: jjkim@snu.ac.kr
Prof. H.-J. Kim
Department of Organic Material Science and Engineering
Pusan National University
2, Busandaehak-ro, Geumjeoung-gu, Busan, Republic of Korea

DOI: 10.1002/adfm.201402321

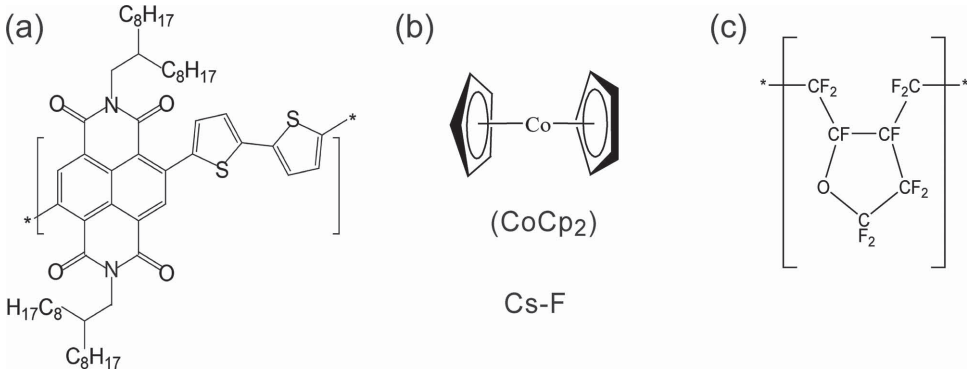

Figure 1. Chemical structure of a) semiconductor: P(NDI2OD-T2); b) dopants: $CoCp_2$ and CsF; and c) dielectric: CYTOP.

to the high-performance p-type polymers, the mobility and stability of NDI-based n-transporting polymers are still in great need of further improvement, e.g., by doping techniques.

Molecular doping in semiconducting layers to induce additional charge carriers has proved as a promising method to enhance conductivity and reduce contact resistance for organic optoelectronic devices such as organic light-emitting diodes (OLEDs) and organic photovoltaics.[9,10] In addition, low concentrations of n-type dopant can also deactivate trap sites.[11,12] However, the application of doping to n-type OFETs calls for two specific and judicious considerations.

The first one is concerned with the microstructure of semiconducting materials. While OLED devices require amorphous semiconductors to prohibit the quenching or recombination of excitons, many organic semiconductors for OFETs possess a crystalline structure to boost carrier mobility. However, the effect of dopants on the crystallinity of the host polymers is still not completely understood, and it should thus be systematically investigated and delicately controlled.[13,14] Molecular patch doping is a good example of a method used to improve device characteristics without influencing the crystallinity of pentacene.[15] However, patch doping can only effectively dope the surface of semiconductors; it cannot affect the bulk conductivity.

The second one is related to the fact that increased conductivity by doping could influence the on–off ratio of the OFET device, which could increase the off current by increasing carrier densities. Low-concentration doping of semiconductor layers and selective doping on/under the contact region have been suggested to maintain the high on–off ratio.[14,16]

To optimize doping materials and techniques for n-type polymeric OFETs, we investigated low-concentration doping in crystalline materials. A representative NDI-based material, P(NDI2DO-T2), was selected for the semiconductor layer due to its high electron-transporting characteristics and acceptable stability for storage in ambient air (**Figure 1**a). The unconventional microstructure of this polymer features weak crystallinity of the out-of-plane direction and predominantly face-on molecular packing along the in-plane direction.[17] In contrast to p-type doping, molecular n-type doping is more difficult, owing to the energetic position of the orbitals required above the LUMO of P(NDI2DO-T2) located at –4.0 eV,[7] which makes the dopant materials unstable against oxygen. Two kinds of strongly reducing and widely used dopants were investigated: an organic compound bis(cyclopentadienyl)-cobalt(II) (cobaltocene, $CoCp_2$) having an ionization energy of 4.0 eV[18] and an alkali metal salt CsF (Figure 1b). To increase operational stability, the CYTOP gate-dielectric insulator was adopted to avoid the hydroxyl trap site for electrons (Figure 1c) and prevent penetration from moisture in the air.[19] Optimized doping of P(NDI2DO-T2) resulted in enhanced n-type mobility, increased on–off ratio, reduced threshold voltage, and increased reliability in bias stress cycles. The key for such optimization is the critical molar ratio (*MR*) of doping, which maintains good crystallinity confirmed by the grazing incidence X-ray diffraction (GIXRD) analysis. We expect this new finding on doping materials and mechanisms can be utilized to further enhance the performance of other n-type polymer FETs and thus pave the way to realize printed complementary circuits.

2. Results and Discussion

2.1. Pristine OFETs

Top-gate, bottom-contact (TGBC) structures of OFETs with pristine P(NDI2DO-T2) films were fabricated via photolithography as they affords large injection areas to lower contact resistance.[20] **Figure 2** shows the schematic structure of the TGBC OFET device and current–voltage characteristics. As compared with the operation at low source–drain voltage V_d (V_d = 20 V), the transfer characteristics (I_d–V_g) at high V_d (V_d = 80 V) exhibited a much higher current at the small V_g region, which signifies an ambipolar regime because of the hole current raised by the potential difference between the gate and drain electrodes. However, the electron current was dominant, as the electron mobility was much higher than the hole mobility (see open dots in Figure 1b and Figure S1 (Supporting Information) for p-type operation). The characteristics of the n-type dominant OFET are also shown in the output curve (I_d vs V_d) in Figure 2c. In the low-V_d regime (V_d < 10 V), the superlinear dependence of I_d on V_d manifests a non-Ohmic injection and a significant contact resistance (R_c) in the injection of electrons. For the n-type regime (V_d = 80 V), we extracted the electron mobility (μ) and threshold voltage (V_{th}) from the saturated regime of the presented device (0.38 cm^2 V^{-1} s^{-1} and 33.5 V, respectively).

We note that the OFETs with pristine film showed a significant hole accumulation regime, which was not observed in some previous references.[21] It indicates that, as compared to the materials used in those references, the materials here probably have the Fermi level relatively further away from the LUMO levels. This difference may cause extra difficulty in electron injection and be responsible for poor injection as observed in the output characteristics.

2.2. Doping Effect: Concentration Dependence

We studied the effect of doping on the current–voltage characteristics of P(NDI2OD-T2) OFETs and compared the two dopants with different doping concentrations (*c*, in weight percent, wt%). The transfer characteristics with various concentrations of $CoCp_2$ and CsF in the semiconductor layers are shown in **Figure 3**a,b, respectively. The effects of doping were examined by extracting the following figures of merit: the on voltage (V_{on}) from which the n-type performance starts to appear, the off current (I_{off}) that is the current at V_{on} (here, the p-type or n-type channel can be still operating, but we still use the term I_{off} for convenience), the threshold voltage (V_{th}), and the mobility (μ) extracted from the saturated regime. As illustrated in Figure 3c, an increase in $CoCp_2$ doping concentration generally leads to a decrease in the positive V_{on} and V_{th}, confirming that the dopants effectively enhance the electron concentration in the channel leading to an earlier turn-on. However, I_{off} firstly decreases until the doping concentration reaches 1 wt% and then increases when the doping concentration increases to 2 wt%. The total current in the ambipolar regime ideally follows (see Supporting Information):

$$|I_d| = I_{n,sat} + I_{p,sat} = \frac{WC_i}{2L}\left[\mu_n\left(V_g - V_{th,n}\right)^2 + \mu_p\left(V_d + V_{th,p} - V_g\right)^2\right] \quad (1)$$

The minimum current at $V_g = V_{on}$ is as follows:

$$\left|I_{off}\left(V_g = V_{on}\right)\right| = \frac{WC_i}{2L}\frac{\mu_n\mu_p}{\mu_n + \mu_p}\left(V_d + V_{th,p} - V_{th,n}\right)^2 \quad (2)$$

where W, L, C_i, and V_d denote channel width, channel length, capacitance of the gate dielectric per unit area, and drain voltage, respectively. The subscripts "n" and "p" denote n-type and p-type, respectively. On the one hand, the negative shift of V_{on} and the decrease in I_{off} (below 1 wt% doping) indicate that the dopants significantly decrease the mobility of the holes and shift the threshold voltage of p-type performance ($V_{th,p}$) toward negative so that the term related to the p-type current decreases. This most likely occurs related to the shift of Fermi level toward LUMO level (away from HOMO level) induced by n-type dopants, because in our previous study on the PCBM film with CsF dopants such shift was clearly evidenced by ultraviolet photoelectron spectroscopy (UPS).[22] The Femi level shift increases the electron concentration but reduces the hole concentration in the semiconductor, therefore increasing hole injection barrier and calling for extra gate voltage to reach mobile states for holes. On the other hand, the increase in I_{off} beyond 1 wt% doping signifies the excess electrons transferred from dopants, which increases the minimum current. Hence, the low doping concentration of $CoCp_2$ guarantees an increased electron concentration and simultaneously keeps a decreased total carrier concentration in the ambipolar or subthreshold regime, leading to a higher on-current level while increasing the on–off ratio with respect to pristine OFETs. Devices with CsF dopants generally show similar trends.

While changes in the parameters V_{on}, I_{off}, and V_{th} follow the usual manner, the values of mobility μ show a rather unanticipated dependence on doping concentration. For $CoCp_2$-doped OFETs, μ increased from 0.38 to 0.67 $cm^2\ V^{-1}\ s^{-1}$ at 0.25 wt% doping and then to 0.72 $cm^2\ V^{-1}$ at 0.50 wt%. However, when additional $CoCp_2$ dopant was added, μ decreased to 0.54 $cm^2\ V^{-1}\ s^{-1}$ at 1 wt% and then to 0.27 $cm^2\ V^{-1}\ s^{-1}$ at 2 wt%. In disordered organic semiconductors with abundant traps, an increase in carrier concentration leads to the filling of trap sites located in the tail states below the mobility edge and thus generally results in a continuously upshifted Fermi level and boosted carrier mobility. The decreased mobility here obviously deviates from such a usual manner. Besides $CoCp_2$, the devices with CsF dopants also exhibit

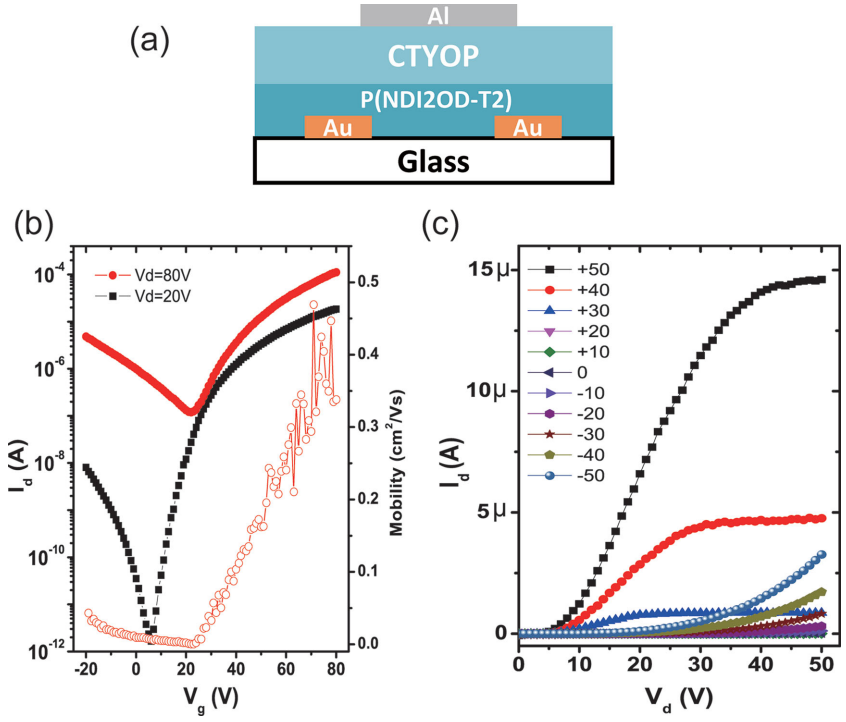

Figure 2. a) Schematic structure of TG/BC OFET device. b) Transfer characteristics of P(NDI2OD-T2) OFET in $V_d = 20$ V, 80 V. Electron and hole mobilities extracted from local slope of square root of I_d against V_g are shown as open dots. c) Output characteristics of P(NDI2OD-T2) OFET in positive V_d region. Applied gate voltages are shown in legend.

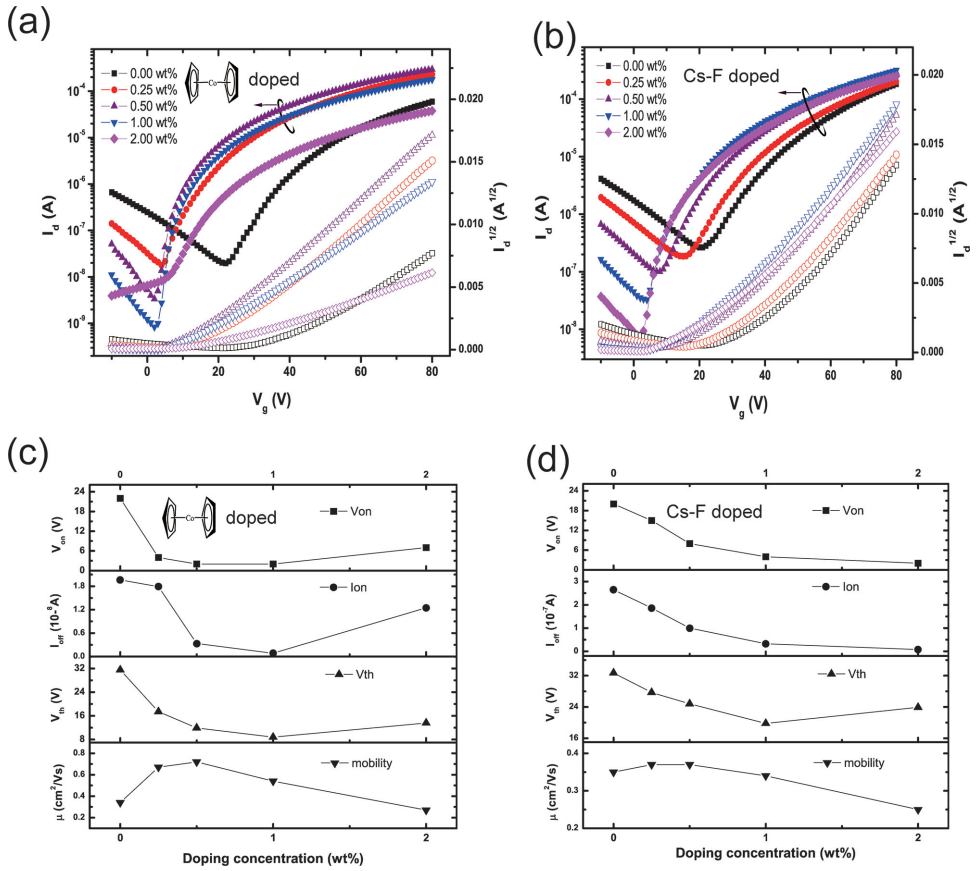

Figure 3. Transfer characteristics of OFETs with various amounts of a) $CoCp_2$ and b) CsF doping to P(NDI2OD-T2) semiconductor layers (V_d = 60 V). Square root of I_d is shown as open dots. Extracted parameters as a function of doping concentration (in wt%) for $CoCp_2$ c) and CsF d) are also shown.

the nonmonotonic dependence of μ on doping concentration, where μ increases slightly and then decreases significantly when doping concentration reaches 1 wt%. The above results are summarized in **Table 1**.

In order to discuss the effect of doping on mobility, we converted the doping concentration c into the MR of dopants (i.e., the number of dopant molecules per monomer in the organic semiconducting (OSC) polymer). The OFET mobilities as a function of MR are shown in **Figure 4**. For both organic and salt dopants, the mobility values increased to their maxima at around $MR \sim 0.03$ and started to decrease beyond it. We compared this result to the report by Olthof et al. who used a dopant similar to $CoCp_2$ in OSC C60 film.[12] In their theoretical and experimental results, at low-doping MR, the charge-transport properties and Fermi-level position were dominated by trap states, and thus, the conductivity and mobility values increased as MR increased. Once the transition point (MR of 10^{-3} to 10^{-2}) was reached, all the traps were filled by dopant-induced charge carriers, the OSC mobility nearly saturated, and the changes in conductivity and Fermi-level position followed standard semiconductor theory.[23] A similar trend with an increase followed by saturation in conductivity has also been reported by Zhang et al.[11] The predicted trends according to these previous findings are depicted as dashed lines in Figure 4. We qualitatively

Table 1. Summary of electrical properties of OFET based on pristine P(NDI2OD-T2) with different doping concentrations.

Doping conc. [wt%]	$CoCp_2$ dopant					CsF dopant				
	V_{on} [V]	I_{off} [A]	On–off ratio	V_{th} [V]	Mobility [$cm^2 V^{-1} s^{-1}$]	V_{on} [V]	I_{off} [A]	On–off ratio	V_{th} [V]	Mobility [$cm^2 V^{-1} s^{-1}$]
0	20	2.6E–07	6.90E+02	32.7	0.35 ± 0.03	20	2.6E–07	6.90E+02	32.7	0.35 ± 0.03
0.25	4	1.8E–08	1.27E+04	17.4	0.67 ± 0.03	15	1.9E–07	1.09E+03	27.7	0.37 ± 0.01
0.5	2	3.3E–09	8.79E+04	11.9	0.72 ± 0.05	8	1E–07	2.92E+03	24.8	0.37 ± 0.02
1	2	8.4E–10	2.14E+05	8.8	0.54 ± 0.03	4	3.3E–08	9.79E+03	19.8	0.34 ± 0.04
2	7	1.3E–08	3.03E+03	13.6	0.27 ± 0.01	2	7.5E–09	3.37E+04	23.9	0.25 ± 0.01

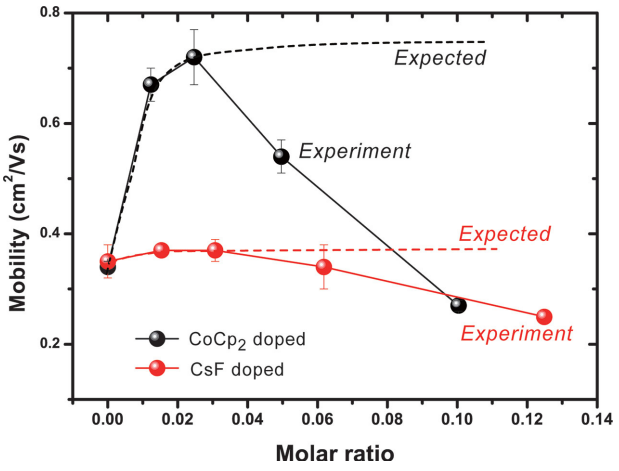

Figure 4. Mobility values as function of doping *MR* for $CoCp_2$ (black) and CsF (red) dopants. Dashed lines are expected trends, sketched by analog to the mobility of C60 film doped with $CoCp_2$.[12]

sketched the "expected" trends about the dependence of mobility on doping ratio, by analog to the mobility of C60 film doped with $CoCp_2$ (obtained by Mote Carlo simulation as well as the experimental data).[12] In contrast, our experimental results feature a decreasing regime beyond $MR \sim 0.03$, which is inconsistent with the usual trap filling and transport mechanism mentioned above. As the transport of OSC can also be vitally affected by structural disorders, especially crystallinity, the contrast can be attributed to structural disordering of the semiconductor film at relatively high-doping *MR*s, which will be examined below.

2.3. Doping Effect: Crystallinity

We investigated the difference in the crystallinity of the pristine and doped P(NDI2OD-T2) films with various concentrations by GIXRD. It has been reported that the P(NDI2OD-T2) films have a face-on molecular packing structure with well-organized intergrain connections,[17] which differs from typical highly crystalline, edge-on conjugated polymers that exhibit a strong lamellar stacking peak in the out-of-plane direction (e.g., polythiophene-based polymers such as PBTTT or P3HT).[24] **Figure 5**a depicts the in-plane XRD patterns of a pristine P(NDI2OD-T2) film, a pure $CoCp_2$ film, and a CsF film. The peak (100) at $Q_{xy} = 0.25$ Å^{-1} (corresponding to *d* spacing of

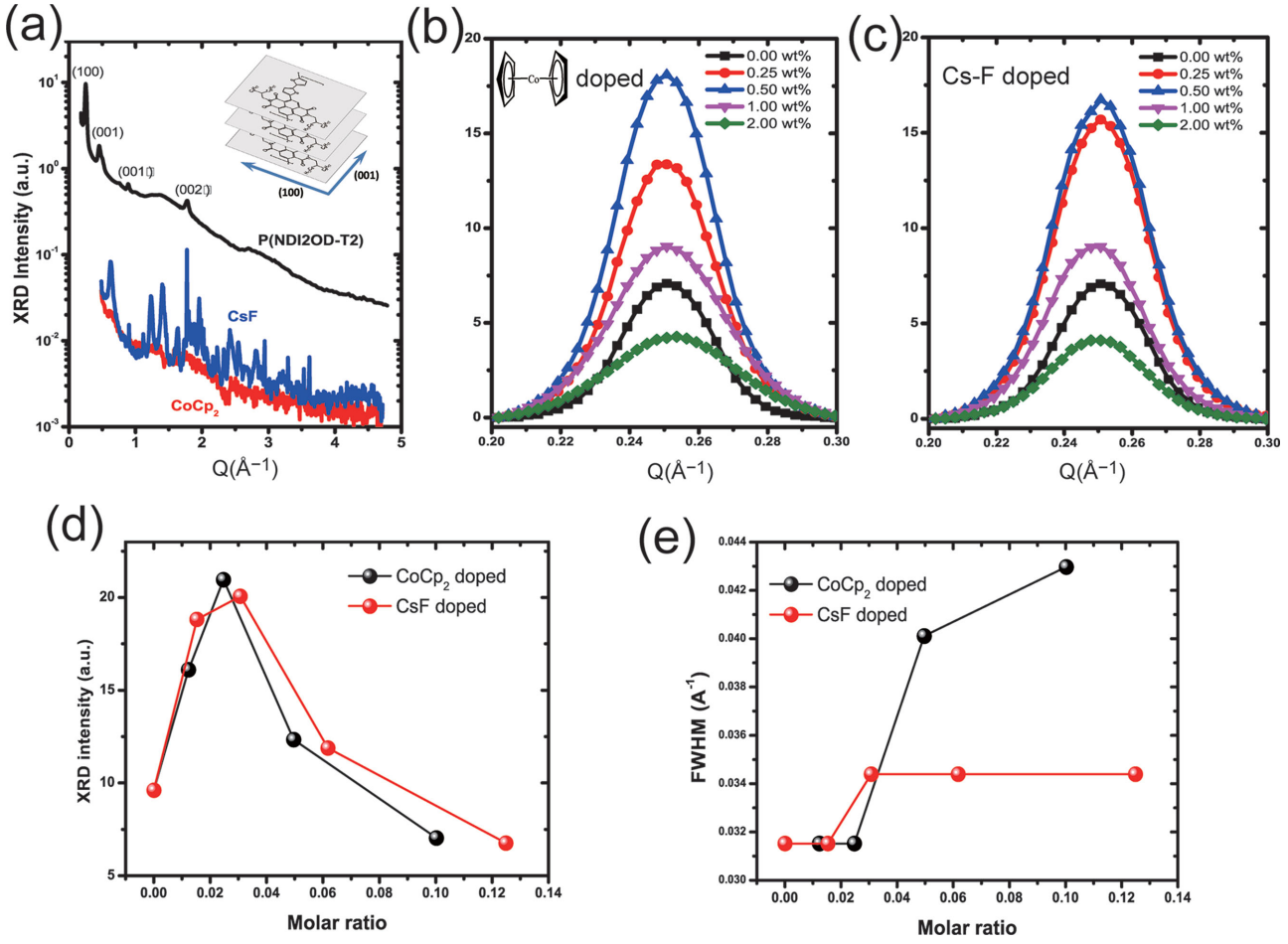

Figure 5. In-plane X-ray diffraction patterns of a) pristine P(NDI2OD-T2), $CoCp_2$, and CsF films in wide range, b) P(NDI2OD-T2) with $CoCp_2$ dopant, and c) P(NDI2OD-T2) with CsF dopant around (100) peak (background subtracted). Inset: a) illustrates face-on crystalline structure of P(NDI2OD-T2). In d) and e), intensities and FWHM of (100) peaks are plotted as function of doping *MR*, respectively.

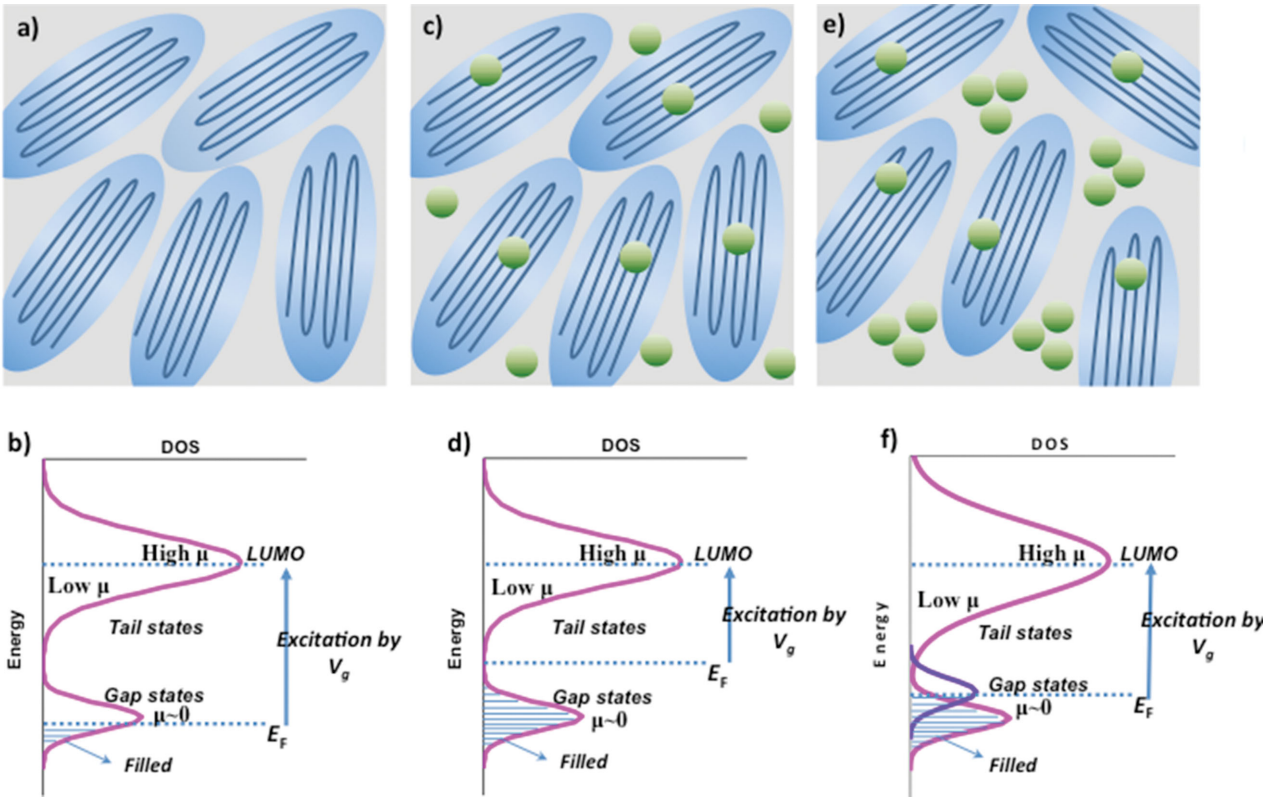

Figure 6. Schematic representation of effect on crystallization and DOS depending on doping ratio: a,b) pristine film; c,d) low doping below critical *MR*; e,f) doping above critical *MR*, leading to disturbed crystallinity and higher degree of disorder in charge transport. In DOS scheme, Fermi level at same V_g is shown relative to center of LUMO to illustrate evolution of gap states (traps where mobility is zero). Different mobilities indicate effect of energetic disorder on mobility and different required V_g for reaching high mobility.

2.5 nm) of the P(NDI2OD-T2) film confirms the in-plane crystalline structure as illustrated by the inset scheme. The (001) and (001′) peaks signify two polymorphs associated with the chain backbone.[17] The evolution of the lamellar stacking peak (100) upon doping of different dopants and concentrations are shown in Figure 5b,c. Both patterns showed the same tendency: the intensity of the peak increased as the doping concentration increased to 0.5 wt% and then decreased with further doping of 1.0 and 2.0 wt%. Using *MR* to compare, we find this trend is clearly observed as an ascending and a descending segment separated at the critical value of doping $MR \sim 0.03$ (Figure 5d). We are not clear why the peak intensity increased from the pristine film up to critical *MR* value. One possibility is that the formation of charge complexes between electron-deficient polymer and electron-rich dopant increases the packing forces to form crystalline domains. Yet only the increased intensity of XRD signals may not give firm evidence on enhanced crystallinity below the critical *MR* value, because the full width of half maximum (FWHM) does not show observable change in this regime. In contrast, FWHM starts to increase noticeably above the critical $MR = 0.03$ (Figure 5e). With much weaker intensities, the (001) peak exhibits a similar trend (Figure S3, Supporting Information). Hence, the decreased peak intensity and the increased FWHM together firmly evidence a decreased order of in-plane crystallinity above the critical *MR*, and also generally correspond well to the mobility trend that decreased from the same *MR* value shown in Figure 4. The out-of-plane X-ray diffraction patterns of the pristine P(NDI2OD-T2), $CoCp_2$, and CsF films are shown in Figure S4 (Supporting Information), where P(NDI2OD-T2) films showed only a weak and broad peak around $Q_z = 1.6$ Å^{-1} (corresponding to out-of-plane stacking). An atomic force microscope (AFM) was also employed to draft the topographic images of P(NDI2OD-T2) films, but we did not observe obvious differences between the pristine films and the films with dopants in the resolution range.

Then, the unanticipated mobility shown in Figure 4 can be explained by dividing it into three regimes, which are schematically illustrated in **Figure 6**. The pristine film has a density of states (DOS) centered on LUMO levels that are transport levels and deeper gap states that are immobile trap states (acceptor-like energy states). Carriers induced by electrostatic coupling need to populate gap states first, causing large V_{on} and V_{th} and low mobility (Figure 6a,b). Then, without disturbing film crystallinity, the initial low doping increases carrier density, fills deep trap states, shifts the Fermi level closer to transport levels (near LUMO level), and enhances the effective mobility, which results in continuous improvement in overall electrical performance in the regime below the critical *MR* (Figure 6c,d). This regime is generally consistent with previous reports and theory.[11,12] Above that *MR*, dopants start to obstruct the

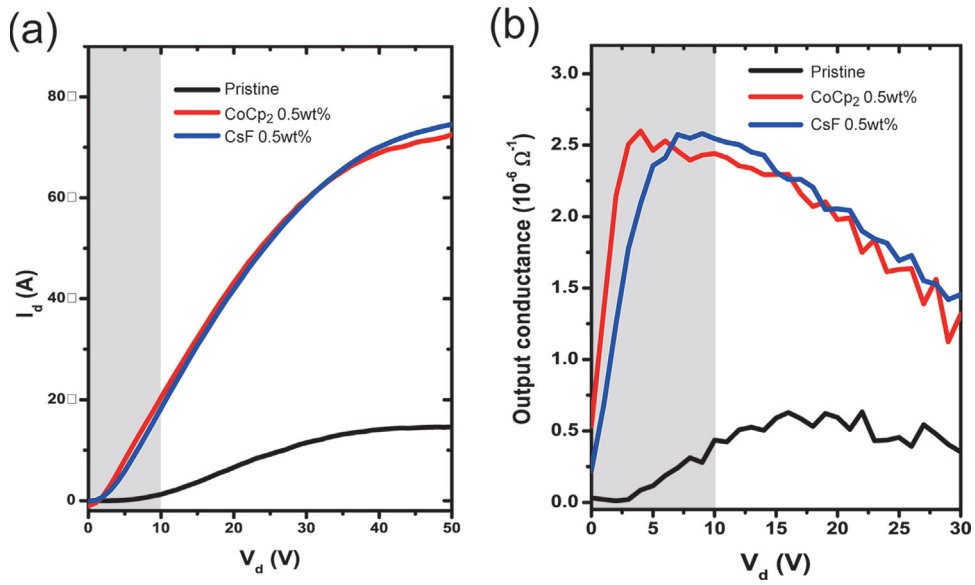

Figure 7. a) Output characteristics of OFETs (V_g = 50 V) with pristine film (black) and films with dopants at concentration of 0.5 wt% (red and blue). b) Output conductance extracted from "a." Gray areas (V_d < 10 V) highlight improved injection after optimized doping.

in-plane crystallization of polymers (Figure 6e), which is probably due to its own aggregation, because we noted that a doping concentration higher than 2 wt% led to the observable aggregation of dopants in film. As electron transport mainly occurs parallel to the substrate, the degraded in-plane structural order deteriorates the electron transport by inducing larger energetic disorder (illustrated as broadened density of mobile states)[25] and extra immobile gap states (illustrated as an extra trap DOS which is qualitatively sketched, Figure 6f). These changes finally result in more trapped charges and manifest in a lower effective mobility. In total, the change of mobility originates from the interplay between the deep-trap filling effect (positive) and crystallization disturbing effect (negative), and the critical *MR* signifies the transition from the positive-effect dominating regime to the negative-effect dominating. Interestingly, for both organic compound $CoCp_2$ and inorganic salt CsF dopants, we observe similar values for the critical *MR*, a relatively low doping ratio (3 molecules of dopants per 100 NDI2OD-T2 monomers). This result highlights the judicious choice of a low-doping ratio and provides a reference value for other dopants or polymers.

2.4. Optimized Doping

Accordingly, an *MR* around 0.03 (0.5 wt% for $CoCp_2$ and CsF) is regarded as the optimized doping ratio that compromises between high excess carrier density and proper crystallinity. In the following, we further demonstrate the benefits of optimized doping in injection properties and operational stability. The output characteristics (I_d–V_d curves at V_g = 50 V) of P(NDI2OD-T2) OFETs with *MR* ~ 0.03 (0.5 wt% concentration) of $CoCp_2$ and CsF are shown in **Figure 7** (see Figure S2 for various values of V_g, Supporting Information). Below V_d = 10 V, I_d of the OFET with a pristine film exhibited a strong nonlinear dependence on V_d, while this effect was much alleviated in those with either dopant (Figure 7a, gray area). Such behavior originates from the large injection barrier ($\Delta\phi$), roughly estimated by the difference between the work function of Au (–4.5 to –4.7 eV) and the LUMO level of polymer P(NDI2OD-T2) (–4.0 eV). Due to the large barrier, a wide depletion region appears next to the drain electrode, which leads to the nonlinear dependence of I_d on V_d. Upon doping, the depletion width W_d is narrowed roughly following $W_d \propto N_D^{1/2}$ (N_D is the dopant density), and the tunneling current increases dramatically (see Supporting Information).[9,26] The improvement can be quantitatively illustrated by extracting the differential output conductance, $g = \partial I_d/\partial V_d$ (Figure 7b). The differential output conductance g of OFETs with either dopant is about 20 times higher than that with pristine film when operating at V_d = 5 V. In addition, g reaches the maximum at about 5 V, compared to 16 V in the reference device. Hence, only 0.03 *MR* (0.5 wt%) induces a highly conductive and fast turn-on channel, which not only enhances current but also allows a three times lower operating voltage. Apparently, doping in conjugated polymers can be combined with solution-processed insertion layers[27] cast on electrodes to further improve injection in future.

The P(NDI2OD-T2) OFETs with dopants also exhibited improved operational stability under cyclic bias stress. We repeated 1000 sweeps from V_g = 0 V to V_g = 60 V with constant V_d = 40 V and collected the data at the interval of 50 times per scan. Because P(NDI2OD-T2) and CYTOP are stable in N_2 atmospheric conditions, the change of electrical characteristics is dominated by bias stress rather than the degradation of materials. **Figure 8**a depicts the change of transfer characteristics for OFET without doping, showing that the current continuously increased as the measurement was repeated. Figure 8b,c shows the transfer characteristics of OFET devices with 0.5 wt% $CoCp_2$ doping and 0.5 wt% CsF doping, respectively. After 1000 cycles, these two devices showed characteristics that had not significantly changed with respect to the first scan.

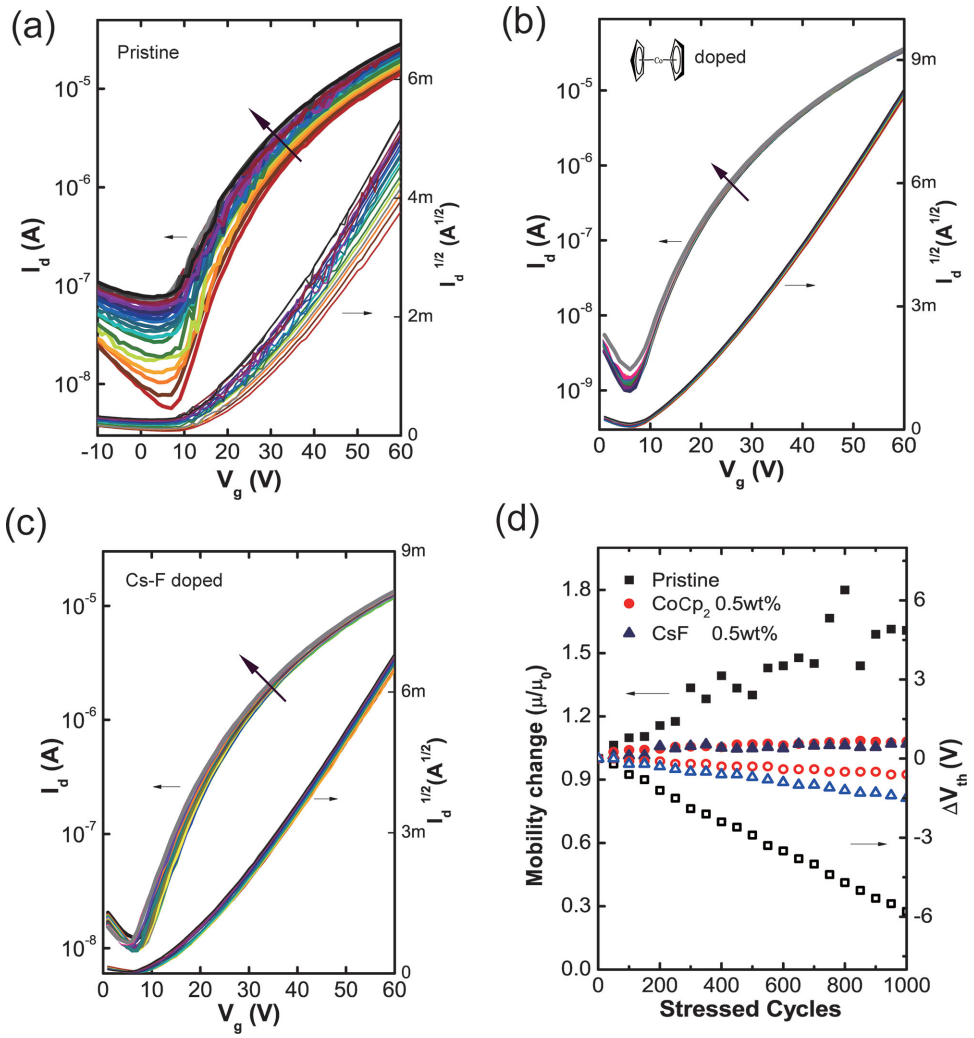

Figure 8. Change of transfer characteristics after bias stress test with a) pristine, b) $CoCp_2$-doped, and c) CsF-doped devices. d) Mobility change and threshold voltage shift with stress cycles.

Figure 8d depicts the extracted mobility and threshold voltage with bias stress as a function of scan times. In the pristine film FET, V_{th} exhibited a shift of 6 V toward positive, and the FET mobility increased about 70% after 1000 cycles of measurement. The positive shift of V_{th} and the increased FET mobility imply that states near the bottom of tail states were continuously filled up (Figure 7b) and were not released during the stress. On the contrary, the devices with optimum dopants featured much better reliability. The changes in V_{th} and μ were no more than 1.5 V and 8%, respectively. The densities of trapped charges per unit area (N_t) were estimated by[28] $N_t = |\Delta V_{th}|\ C_i/q$. Here, q is the elementary charge, and ΔV_{th} is the shift of V_{th}. Correspondingly, N_t values of pristine, $CoCp_2$-doped, and CsF-doped P(NDI2OD-T2) after 1000 bias cycles were 2.3×10^{12}, 2.4×10^{11}, and 6×10^{11} cm^{-2}, respectively. In accordance with Figure 7d, the improved reliability originates from the free electrons that are generated by strong electron-donating $CoCp_2$ or CsF, which are transferred to semiconducting polymers and then occupy trap states.

3. Conclusion

In conclusion, we have investigated the doping effect on the characteristics of solution-processed, n-type polymer P(NDI2OD-T2) OFETs with various concentrations of the electron donor $CoCp_2$ and CsF. The OFETs with an optimized, low *MR* of dopants exhibited simultaneously improved mobility (two times higher), on–off ratio (100 times higher), injection, and reliability. The remarkable enhancement results from the optimization of carrier density and crystallization obtained at the critical values of *MR*, at which mobility reached the maximum. Beyond the critical *MR*, the crystallinity of the semiconducting polymer was degraded so that the transport was deteriorated by structural disorders. The results on the doping mechanism provide a simple and effective method to achieve high-performance n-type polymer FETs and generally benefit solution-processed, organic, and printing electronics. When using other semiconducting polymers or device configuration, we expect the similar effect would probably occur upon doping,

as dopants can heal deep traps in band-gap and yet affect the crystallization to change charge transport properties.

4. Experimental Section

The source and drain electrodes were Cr/Au (3 nm/27 nm) patterned on glass substrate. The channel length and width were 10 and 1000 μm, respectively. The dopants $CoCp_2$ and CsF were purchased from Sigma-Aldrich without any purification. Small quantities of $CoCp_2$ and CsF dopants were dissolved in 2-ethoxyethanol and mixed with P(NDI2DO-T2) dissolved in p-xylene with the following weight ratios: 0.0%, 0.025%, 0.5%, 1.0%, and 2.0%. A higher mixing ratio led to the aggregation of dopants on the films. Doped P(NDI2DO-T2) was deposited by spin casting and dried at 110 °C. The thickness of the spin-cast film measured by a PSIA XE-100 AFM was 30 nm. CYTOP was selected for the dielectric insulator, because its hydroxyl-free interface can reduce trap sites and increase device stability. This was also an important reason to ensure that perfluorotrialkylamine, the solvent of CYTOP, was an orthogonal solvent to P(NDI2DO-T2) and the dopant molecules. CYTOP was deposited by spin casting with 500-nm thickness and annealed at 130 °C for 1 Hr. All the spin-casting processes were performed in an N_2 atmosphere in a glove box. The Al (50 nm) gate electrode was deposited by thermal evaporation through a shadow mask in a high vacuum condition. The electrical characteristics of the devices were measured with an Agilent 4156A Semiconductor Parameter Analyzer in an N_2 atmosphere. The capacitance of the CYTOP insulator was 3.7×10^{-9} F cm^{-2}, and the FET mobility was calculated in the saturation regime extrapolating the slope of I_d versus V_g curves:

$$I_{d,Sat} = \frac{W}{2L} C_i \mu \left(V_g - V_{th,n}\right)^2 \quad (3)$$

The hole mobility in the ambipolar regime (Figure 2b) was extracted by

$$I_{d,Sat} = \frac{W}{2L} C_i \mu_p \left(V_g - V_{th,n} - V_d\right)^2 \quad (4)$$

The bias stress was applied to investigate operational stability with 1000 gate bias sweeps in an N_2 atmosphere. This measurement was done within 8 h, so degradation of the semiconductor molecules was not taken into account.

The molar masses (M) of $CoCp_2$, CsF, and monomer NDI2DO-T2 were 189.12, 151.9, and 929.37 g mol^{-1}, respectively. We then converted the doping concentration c into the MR of dopants:

$$MR = \frac{c / M_{dop}}{(1-c) / M_{OSC}} \quad (5)$$

where M_{dop} and M_{osc} denote the molar mass of the dopant molecule (CoCp2 or CsF) and the monomer of the OSC polymer (a single unit of NDI2OD-T2), respectively.

In order to investigate the structure of P(NDI2DO-T2), GIXRD measurements were carried out at the 5C beam line at the Pohang Accelerator Laboratory (PAL), Korea. The samples for X-ray measurement were fabricated on soda-lime bare glass. The semiconducting P(NDI2DO-T2) material with dopants was spin-cast and dried under the same conditions as the OFET samples. Scattering data were plotted as a function of the scattering vector Q, where Q_{xy} and Q_z were the components of the scattering vector in-plane and out-of-plane (i.e., parallel and perpendicular to the substrate), respectively. The d spacing was obtained by $d = 2\pi/Q$ (in Å), where Q was the peak position.

Supporting Information

Supporting Information is available from the Wiley Online Library or from the author.

Acknowledgements

C.L. and J.J. contributed equally to this work. This work was supported by the National Research Foundation of Korea (NRF) grant funded by the Korean Government (MSIP) (NRF-2014R1A2A2A01007159), the Center for Advanced Soft Electronics funded by the Ministry of Science, ICT, and Future Planning as a Global Frontier Project (2013M3A6A5073183), and the Dongguk University Research Fund of 2014. This work was also supported by the grant from National "985" (30000-31101200) and Shunde Government on SYSU-CMU Joint Research Institute, Guangdong.

Received: July 14, 2014
Revised: November 12, 2014
Published online: December 23, 2014

[1] K.-J. Baeg, M. Caironi, Y.-Y. Noh, *Adv. Mater.* **2013**, *25*, 4210.
[2] B. Sun, W. Hong, Z. Yan, H. Aziz, Y. Li, *Adv. Mater.* **2014**, *26*, 2636.
[3] C. B. Nielsen, M. Turbiez, I. McCulloch, *Adv. Mater.* **2013**, *25*, 1859.
[4] a) H. Chen, Y. Guo, G. Yu, Y. Zhao, J. Zhang, D. Gao, H. Liu, Y. Liu, *Adv. Mater.* **2012**, *24*, 4618; b) Z. Chen, M. J. Lee, R. Shahid Ashraf, Y. Gu, S. Albert-Seifried, M. Meedom Nielsen, B. Schroeder, T. D. Anthopoulos, M. Heeney, I. McCulloch, *Adv. Mater.* **2012**, *24*, 647; c) J. S. Lee, S. K. Son, S. Song, H. Kim, D. R. Lee, K. Kim, M. J. Ko, D. H. Choi, B. Kim, J. H. Cho, *Chem. Mater.* **2012**, *24*, 1316; d) H.-W. Lin, W.-Y. Lee, W.-C. Chen, *J. Mater. Chem.* **2012**, *22*, 2120; e) J. D. Yuen, J. Fan, J. Seifter, B. Lim, R. Hufschmid, A. J. Heeger, F. Wudl, *J. Am. Chem. Soc.* **2011**, *133*, 20799; f) H.-R. Tseng, H. Phan, C. Luo, M. Wang, L. A. Perez, S. N. Patel, L. Ying, E. J. Kramer, T.-Q. Nguyen, G. C. Bazan, A. J. Heeger, *Adv. Mater.* **2014**, *26*, 2993.
[5] H. T. Nicolai, M. Kuik, G. A. H. Wetzelaer, B. de Boer, C. Campbell, C. Risko, J. L. Brédas, P. W. M. Blom, *Nat. Mater.* **2012**, *11*, 882.
[6] a) H. Yan, Z. Chen, Y. Zheng, C. Newman, J. R. Quinn, F. Dötz, M. Kastler, A. Facchetti, *Nature* **2009**, *457*, 679; b) M. Caironi, M. Bird, D. Fazzi, Z. H. Chen, R. Di Pietro, C. Newman, A. Facchetti, H. Sirringhaus, *Adv. Funct. Mater.* **2011**, *21*, 3371.
[7] G.-J. A. Wetzelaer, M. Kuik, Y. Olivier, V. Lemaur, J. Cornil, S. Fabiano, M. A. Loi, P. W. Blom, *Phys. Rev. B* **2012**, *86*, 165203.
[8] R. Kim, P. S. Amegadze, I. Kang, H. J. Yun, Y. Y. Noh, S. K. Kwon, Y. H. Kim, *Adv. Funct. Mater.* **2013**, *23*, 5719.
[9] K. Walzer, B. Maennig, M. Pfeiffer, K. Leo, *Chem. Rev.* **2007**, *107*, 1233.
[10] a) D.-S. Leem, H.-D. Park, J.-W. Kang, J.-H. Lee, J. W. Kim, J.-J. Kim, **2007**, *91*, 011113; b) J.-H. Lee, D.-S. Leem, H.-J. Kim, J.-J. Kim, *Appl. Phys. Lett.* **2009**, *94*, 123306.
[11] Y. Zhang, B. de Boer, P. W. Blom, *Phys. Rev. B* **2010**, *81*, 085201.
[12] S. Olthof, S. Mehraeen, S. K. Mohapatra, S. Barlow, V. Coropceanu, J.-L. Brédas, S. R. Marder, A. Kahn, *Phys. Rev. Lett.* **2012**, *109*, 176601.
[13] a) P. Wei, J. H. Oh, G. Dong, Z. Bao, *J. Am. Chem. Soc.* **2010**, *132*, 8852; b) C. Y. Chan, C. Chow, S. So, *Org. Electron.* **2011**, *12*, 1454; c) J. S. Swensen, L. Wang, J. E. Rainbolt, P. K. Koech, E. Polikarpov, D. J. Gaspar, A. B. Padmaperuma, *Org. Electron.* **2012**, *13*, 3085.
[14] L. Ma, W. H. Lee, Y. D. Park, J. S. Kim, H. S. Lee, K. Cho, *Appl. Phys. Lett.* **2008**, *92*, 063310.
[15] J. H. Kim, S. W. Yun, B.-K. An, Y. D. Han, S.-J. Yoon, J. Joo, S. Y. Park, *Adv. Mater.* **2013**, *25*, 719.
[16] a) P. Wei, T. Menke, B. D. Naab, K. Leo, M. Riede, Z. Bao, *J. Am. Chem. Soc.* **2012**, *134*, 3999; b) J. H. Oh, P. Wei, Z. Bao, *Appl. Phys. Lett.* **2010**, *97*, 243305.
[17] J. Rivnay, M. F. Toney, Y. Zheng, I. V. Kauvar, Z. Chen, V. Wagner, A. Facchetti, A. Salleo, *Adv. Mater.* **2010**, *22*, 4359.

[18] C. K. Chan, F. Amy, Q. Zhang, S. Barlow, S. Marder, A. Kahn, *Chem. Phys. Lett.* **2006**, *431*, 67.
[19] J. Jang, J. W. Kim, N. Park, J.-J. Kim, *Org. Electron.* **2008**, *9*, 481.
[20] K.-J. Baeg, D. Khim, S.-W. Jung, M. Kang, I.-K. You, D.-Y. Kim, A. Facchetti, Y.-Y. Noh, *Adv. Mater.* **2012**, *24*, 5433.
[21] M. Caironi, C. Newman, J. Moore, D. Natali, H. Yan, A. Facchetti, H. Sirringhaus, *Appl. Phys. Lett.* **2010**, *96*, 183303.
[22] D. Khim, K.-J. Baeg, M. Caironi, C. Liu, Y. Xu, D.-Y. Kim, Y.-Y. Noh, *Adv. Funct. Mater.* **2014**.
[23] Y. Zhang, P. W. M. Blom, *Appl. Phys. Lett.* **2011**, *98*, 143504.
[24] a) T. Schuettfort, B. Watts, L. Thomsen, M. Lee, H. Sirringhaus, C. R. McNeill, *ACS Nano* **2012**, *6*, 1849; b) B. O'Connor, R. J. Kline, B. R. Conrad, L. J. Richter, D. Gundlach, M. F. Toney, D. M. DeLongchamp, *Adv. Funct. Mater.* **2011**, *21*, 3697.
[25] R. Noriega, J. Rivnay, K. Vandewal, F. P. Koch, N. Stingelin, P. Smith, M. F. Toney, A. Salleo, *Nat. Mater.* **2013**, *12*, 1038.
[26] S. Olthof, W. Tress, R. Meerheim, B. Lüssem, K. Leo, *J. Appl. Phys.* **2009**, 103711.
[27] J. Meyer, R. Khalandovsky, P. Gorrn, A. Kahn, *Adv. Mater.* **2011**, *23*, 70.
[28] a) K. Pernstich, S. Haas, D. Oberhoff, C. Goldmann, D. Gundlach, B. Batlogg, A. Rashid, G. Schitter, *J. Appl. Phys.* **2004**, *96*, 6431; b) J. A. Letizia, J. Rivnay, A. Facchetti, M. A. Ratner, T. J. Marks, *Adv. Funct. Mater.* **2010**, *20*, 50.